Parametric Study for α-$CsPbI_2Br$ Film Growth by Mist Chemical Vapor Deposition

Jeha Kim*

Department of Energy Convergence Engineering, Cheongju University, Eumseoung-gun, Chungbuk 27739, Republic of Korea

Research Article

Received: 14-Oct-2024, Manuscript No. JPAP-24-150078; **Editor assigned:** 16-Oct-2024, Pre QC No. JPAP-24-150078 (PQ); **Reviewed:** 30-Oct-2024, QC No. JPAP-24-150078; **Revised:** 05-Mar-2025, Manuscript No. JPAP-24-150078 (R); **Published:** 12-Mar-2025, DOI: 10.4172/2320-2459.13.1.007

***For Correspondence:** Jeha Kim, Department of Energy Convergence Engineering, Cheongju University, Eumseoung-gun, Chungbuk 27739, Republic of Korea;
E-mail: jeha@cju.ac.kr

Citation: Kim J. Parametric Study for α-$CsPbI_2Br$ Film Growth by Mist Chemical Vapor Deposition. RRJ Pure Appl Phys. 2025;13:007.

ABSTRACT

Using an atmospheric mist Chemical Vapor Deposition (CVD), we fabricated successfully $CsPbI_2Br$ films under various growth conditions: $CsPbI_2Br$ precursor of 0.4 molar concentration, carrier and dilution N_2 flow rates of 200 and 1500 cc/min, substrate temperature of 68°C, and growth time of 35 min.

Keywords: Atmospheric mist chemical vapor deposition; Perovskite crystalline growth; Molar concentration ratio; Growth temperature; N_2 gas flow rate

INTRODUCTION

Currently, perovskite solar cells have garnered considerable attention because of their high efficiency of up to 25.2% [1], low cost, and simple process, which allow their commercial applications [2-5]. Perovskites are composed of organic volatile molecules that induce to form hydro-compounds with the moisture in air [6-8]. To reduce such degradation in air, inorganic cation Cs^+ is used to form purely inorganic $CsPbX_3$ (X=I, Br) for stability [9-11]. Under a humid environment, α-$CsPbI_2Br$ has relatively stable bandgap energy of 1.92 eV and transforms the dark phase with low bandgap to the yellow phase with high bandgap energy of 2.85 eV [12]. Among various methods [13-19], pseudo-CVD is known as a new approach proposed for perovskite film preparation that uses microscopic mists of a solution, referred to as mist CVD.

As for preparing high quality cubic α-$CsPbI_2Br$ films by mist CVD, in this report, we investigated systematically the film preparation with various parameters and optimized them.

MATERIALS AND METHODS

Sample preparation

Figure 1 is a schematic of mist CVD with the reactor channel heated at the bottom. The aerosol mist generated ultrasonically is directed to the reactor by N_2 gas (99.8%). $CsPbI_2Br$ precursor solution was prepared using Cesium Bromide (CsBr, 99.999%) and lead (II) iodide (PbI_2, 99.999%) at different molar concentrations in a mixed solvent with 4:1 (v/v%) N, N-dimethylformamide (DMF, 99.8%) and Dimethyl Sulfoxide (DMSO, ≥ 99.9%). Then $CsPbI_2Br$ precursor was stirred for 7 h at 70°C inside a N_2 glove box. An ultrasonically generated microscopic mist droplet is then transferred into the reactor using N_2 gas and flows through a rectangular channel of 3 mm × 108 mm × 180 mm. Inside the reactor, the perovskite grain nucleates while heating and crystallizes followed by post-annealing [20]. Table 1 shows a summary of the experimental parameters for the growth study. The details will be found in the previous report [21].

Figure 1. (a) Schematic of the mist CVD process and (b) Photo of instrument.

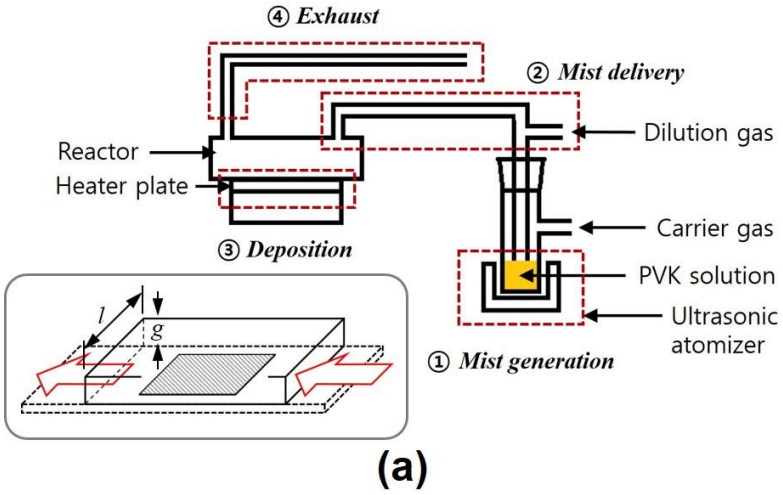

Table 1. Combination of parameters of the $CsPbI_2Br$ film growth.

Parameters (unit)	Values
Concentration of precursor (Mole)	0.2/0.4/0.6
Growth temperature, T_{sub} (°C)	72/68/60
Growth time, t_G (min)	35/35/30
Flow rate of carrier, Q_c (cc/min)	150/200/225
Flow rate of dilution, Q_d (cc/min)	1300/1500/1700

RESULTS AND DISCUSSION

As shown in Figure 2 (a-c), the FE-SEM images of the films with precursors of 0.2, 0.4, and 0.6 M exhibit a smooth surface with an exception of 0.2 M sample having voids and nodules on the film. Figure 2 (d) shows the X-ray diffraction spectrum for the samples of 0.4 M produced the reflections at 14.68°, 20.94°, and 29.68° corresponding to the cubic α-$CsPbI_2Br$ (100), (110), and (200) planes, respectively [22,23].

Figure 2. FE-SEM images of the $CsPbI_2Br$ with Q_c=150 cc/min and Q_d=1500 cc/min: (a) 0.2 M, T_{sub}=72°C, t_G=35 min; (b) 0.4 M, T_{sub}=68°C, t_G=35 min, (c) 0.6 M, T_{sub}=60°C, t_G=30 min, (d) XRD spectrum for 0.2 M sample.

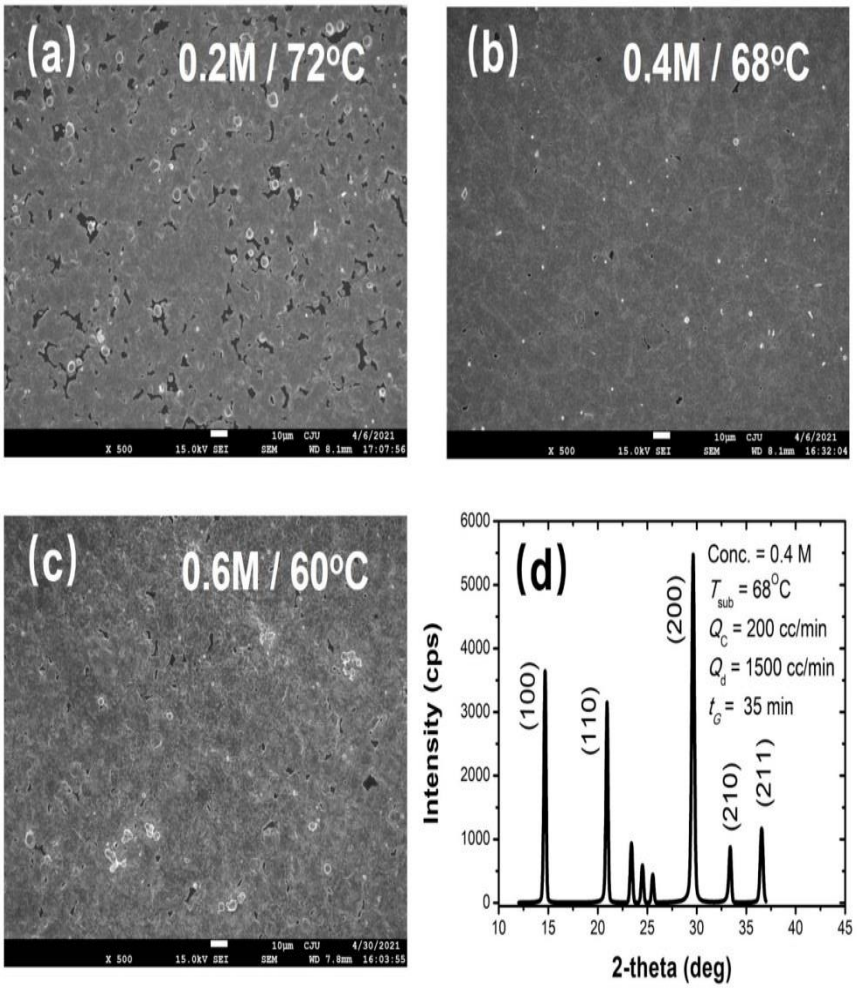

Figure 3 shows that the optical transmittance exhibits little variation for the wavelength λ=350-650 nm and increased rapidly at >650 nm. The optical bandgap energy E_g estimated from the Tauc plot [24] was 1.914 eV (λ_g of ~648 nm) (inset) that agrees with the bulk value of the α-$CsPbI_2Br$ crystal.

Figure 3. Optical transmittance spectra with an inset of their Tauc plots.

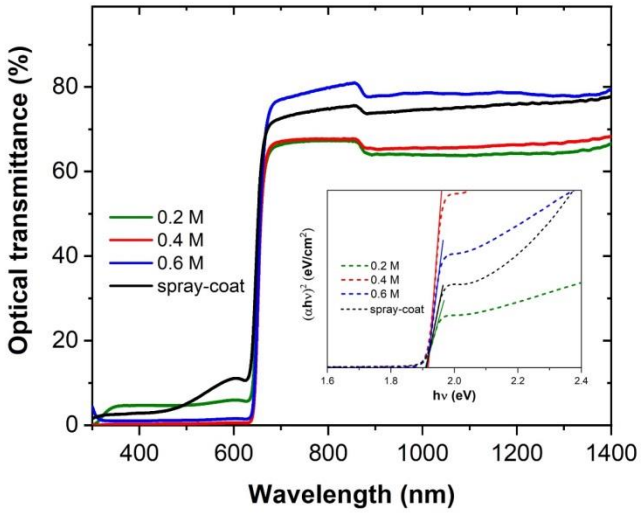

The amount of mist generation and transfer was dependent on the flow rates Q's of N_2 gas. A ratio of the carrier Q_c to dilution Q_d gas flow rates R appears an important factor for the film growth: R ~1/10. For a successful film growth with smooth and defect-free surface, Q_c should be set over a threshold of 200 cc/min as shown in Figure 4 (a) and (b). As Q_d increases, the individual voids generated increase slightly; $Q_d \cong 1500$ cc/min.

Figure 4. FE-SEM images of the samples with 0.4 M, T_{sub}=68°C, t_G=35 min, N_2 gas (Q_c, Q_d): (a) 200 cc/min, 1300 cc/min; (b) 200 cc/min, 1500 cc/min and the samples with Q_c=200 cc/min, and Q_d=1500 cc/min and different T_{sub}; (c) 66°C, (d) 68°C.

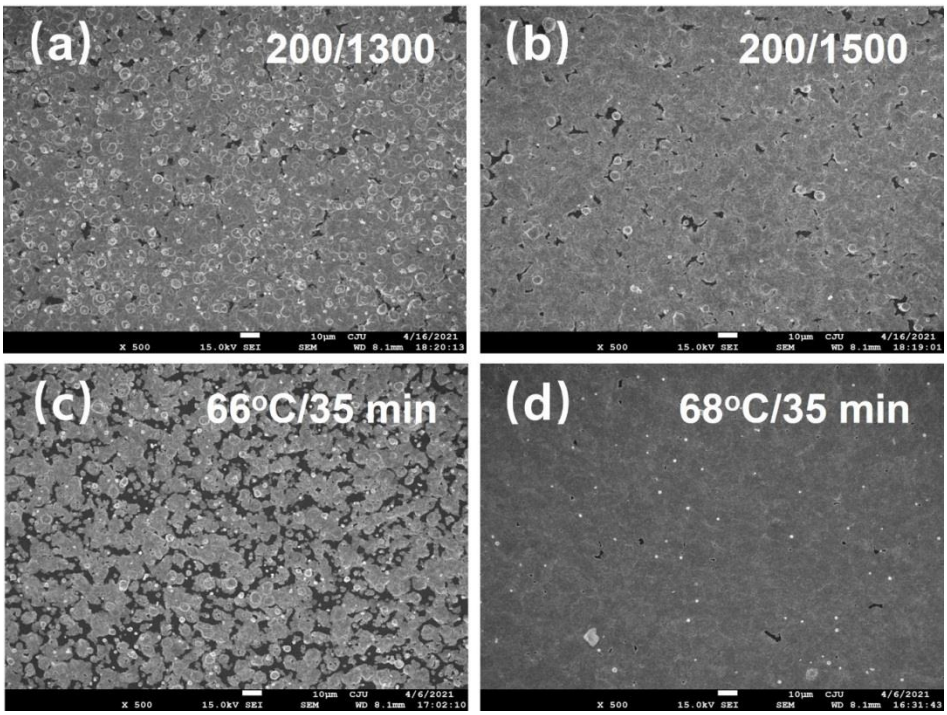

It was found that the surface morphology of the film is significantly affected by the substrate temperature T_{sub}. The surface coverage of the grains is improved dramatically as T_{sub} increased only by 2°C from T_{sub}=66°C to 68°C as exhibited in Figure 4 (c) and (d). At a higher T_{sub}, the film cannot be formed because the mist of the solution is dried and evacuated. At

T_{sub}=68°C, the perovskite film exhibits the best quality with complete grains covered with smooth surfaces, minimal defect density of voids, and the lowest optical transmittance.
In addition, the growth exhibits drastic changes in the surface morphology with the growth time t_G. As t_G increases from 25 min to 30 min, the grains suddenly covered the entire surface and the voids disappeared in the surface, while the overall film thickness remained the same as for t_G=25 min; t=1.82~2.38 μm.
For the perovskite film growth by mist CVD, it was crucial to stabilize the growth parameters while growing the perovskite films on the heated substrate. This observation implies that the film growth with time is strongly influenced by the nucleation of the crystal from the liquidous phase to a solid in the mist CVD process under the reactor environment.

CONCLUSION

In summary, using the mist CVD method we successfully prepared the growth of inorganic perovskite films verified with variety of characterization. All the samples exhibit well-defined α-$CsPbI_2Br$ crystal with E_g=1.914 eV. It was crucial to maintain the growth conditions at a narrow operation tolerance such that the amount of precursor mist was stabilized inside the reactor with the gas ratio R~1/10 at the temperature t_G=68°C.

ACKNOWLEDGEMENTS

This research was financially supported by the Ministry of Trade, Industry and Energy, Korea, under the “Regional Innovation Cluster Development Program s(R and D) (P0025862)” supervised by the Korea Institute for Advancement of Technology (KIAT). This work was supported by a Chungcheongbuk-do and Chungbuk Technopark, A Study on the Accelerator Device Leading Technology Development in 2023 (SR230105).

REFERENCES

1. Sahli F, et al. Fully textured monolithic perovskite/silicon tandem solar cells with 25.2% power conversion efficiency. Nat Mater. 2018;17:820-826.
2. Yang M, et al. Perovskite ink with wide processing window for scalable high-efficiency solar cells. Nat Energy. 2017;2:1-9.
3. Verma A, et al. Towards industrialization of perovskite solar cells using slot die coating. J Mater Chem C. 2020;8:6124-6135.
4. Rezaee E, et al. A route towards the fabrication of large-scale and high-quality perovskite films for optoelectronic devices. Sci Rep. 2022;12:7411.
5. Wojciechowski K, et al. Industrial opportunities and challenges for perovskite photovoltaic technology. Solar RRL. 2019;3:1900144.
6. Ahmad S, et al. *In situ* intercalation dynamics in inorganic–organic layered perovskite thin films. ACS Appl Mater Interfaces. 2014;6:10238-10247.
7. Leijtens T, et al. Overcoming ultraviolet light instability of sensitized TiO_2 with meso-superstructured organometal tri-halide perovskite solar cells. Nat Commun. 2013;4:2885.
8. Juarez-Perez EJ, et al. Thermal degradation of $CH_3NH_3PbI_3$ perovskite into NH_3 and CH_3I gases observed by coupled thermogravimetry–mass spectrometry analysis. Energy Environ Sci. 2016;9:3406-3410.
9. Nam JK, et al. Potassium incorporation for enhanced performance and stability of fully inorganic cesium lead halide perovskite solar cells. Nano Lett. 2017;17:2028-2033.
10. Wang Y, et al. Bifunctional stabilization of all-inorganic α-$CsPbI_3$ perovskite for 17% efficiency photovoltaics. J Am Chem Soc. 2018;140:12345-12348.
11. Liu C, et al. Ultra-thin MoO_x as cathode buffer layer for the improvement of all-inorganic $CsPbIBr_2$ perovskite solar cells. Nano Energy. 2017;41:75-83.
12. Mariotti S, et al. Stability and performance of $CsPbI_2Br$ thin films and solar cell devices. ACS Appl Mater Interfaces. 2018;10:3750-3760.
13. Yang F, et al. Improved interface of $ZnO/CH_3NH_3PbI_3$ by a dynamic spin-coating process for efficient perovskite solar cells. RSC Adv. 2017;7:19030-19038.
14. Dong C, et al. A green anti-solvent process for high performance carbon-based $CsPbI_2Br$ all-inorganic perovskite solar cell. Solar RRL. 2018;2:1800139.

15. Bishop JE, et al. Development of spray-coated perovskite solar cells. ACS Appl Mater Interfaces. 2020;12:48237-48245.
16. Hsu HC, et al. Long-term stable perovskite solar cells prepared by doctor blade coating technology using bilayer structure and non-toxic solvent. Org Electron. 2022;101:106400.
17. Liu M, et al. Efficient planar heterojunction perovskite solar cells by vapour deposition. Nature. 2013;501:395-398.
18. Pammi SV, et al. Predominant stable $MAPbI_3$ films deposited *via* chemical vapor deposition: stability studies in illuminated and darkened states coupled with temperature under an open-air atmosphere. ACS Appl Energy Mater. 2018;1:3301-3312.
19. Wang M, et al. Film fabrication of perovskites and their derivatives for photovoltaic applications *via* chemical vapor deposition. ACS Appl Energy Mater. 2021;5:5434-5448.
20. Haruta Y, et al. One-step coating of full-coverage $CsPbBr_3$ thin films *via* mist deposition for all-inorganic perovskite solar cells. ACS Appl Energy Mater. 2020;3:11523-11528.
21. Kim J, et al. Parametric dependence of $CsPbI_2Br$ perovskite film growth using a mist chemical vapor deposition method. Curr Appl Phys. 2024;60:1-8.
22. Roose B, et al. Critical assessment of the use of excess lead iodide in lead halide perovskite solar cells. J Phys Chem Lett. 2020;11:6505-6512.
23. Hovish MQ, et al. Crystallization kinetics of rapid spray plasma processed multiple cation perovskites in open air. J Mater Chem A. 2020;8:169-176.
24. Tauc J, et al. Optical properties and electronic structure of amorphous Ge and Si. Mater Res Bull. 1968;3:37-46.